CSIRO
Marine Laboratories

REPORT 183

Seasonal Cycles of Steric Sea Level off Western Australia with Error Analysis

K. R. Ridgway

1986

COMMONWEALTH SCIENTIFIC AND INDUSTRIAL RESEARCH ORGANIZATION
MARINE RESEARCH LABORATORIES
GPO BOX 1538, HOBART, TAS. 7001, AUSTRALIA

National Library of Australia Cataloguing-in-Publication Entry

Ridgway, K. R. (Ken R.).

Seasonal cycles of steric sea level off Western Australia with error analysis.

ISBN 0 643 03966 X.

1. Ocean currents—Indian Ocean. 2. Ocean currents—Indian Ocean—Measurement. 3. Ocean circulation—Indian Ocean—Measurement. 4. Sea level—Indian Ocean—Measurement. I. Commonwealth Scientific and Industrial Research Organization (Australia). Marine Laboratories. II. Title. (Series: Report (Commonwealth Scientific and Industrial Research Organization (Australia). Marine Laboratories); no. 183).

551.47'775

86.532-550

SEASONAL CYCLES OF STERIC SEA LEVEL OFF WESTERN AUSTRALIA WITH ERROR ANALYSIS

K. R. RIDGWAY

Division of Oceanography
CSIRO Marine Laboratories
GPO Box 1538, Hobart, Tasmania, 7001
Australia

CSIRO Marine Laboratories Report No. 183

Abstract

Expendable bathythermograph (XBT) data collected within the region 10°-40°S and 105°-130°E, between 1950-1980, are used with T-S relationships and regression estimates of steric height at 450 db relative to 1300 db to obtain estimates of steric sea level relative to 1300 db. These steric sea level data are merged with steric sea levels relative to 1300 db estimated from hydrology observations. Within each of a number of spatial "bins" chosen to best represent known features of the circulation off Western Australia (including the Leeuwin Current), 2-harmonic seasonal curves are fitted to the steric sea level observations. The monthly root mean square deviation of these curves from the true seasonal curve are estimated using a multiple linear regression technique in which both the non-uniform distribution of the data in time and the presence of a correlation between non-seasonal components are considered. Displays of annual mean and bimonthly steric topographies at the 0, 100, 200 and 300 db surfaces (relative to 1300 db) obtained from these 2 harmonic seasonal curves show the seasonal variation of the Leeuwin Current.

1. INTRODUCTION

Over a long period, a variety of observations have suggested that some form of poleward flow exists off the Western Australian coast (Saville-Kent, 1897, Schott 1933, Rochford 1969, Gentilli 1972, Colborn 1975, Andrews 1977). This was not always recognised at the time and it is only very recently that a more complete picture of the Leeuwin Current has emerged; as a narrow, rapid seasonally variable, poleward flowing current along the continental shelf (Cresswell and Golding 1980, Legeckis and Cresswell 1981, Thompson 1984) and which is now known as the Leeuwin Current. This is in sharp contrast to the broad, diffuse, slow moving equatorward flow found on other eastern ocean boundaries (Fofonoff 1962).

The only study of the mean seasonal geostrophic circulation off Western Australia (Wyrtki 1971) gives maps of steric height relative to 1000 db. These show almost no sign of the Leeuwin Current because the hydrology data upon which they are based provided no coverage of the inner part of the continental slope. Several synoptic or near synoptic steric height maps have been reported (Wyrtki 1961a, Hamon 1965, 1972; Andrews 1977; Thompson 1984). The latter two reveal the presence of a strong southward flow associated with the Leeuwin Current but both of them being limited in regional and temporal extent do not provide information on the large scale environment of the Leeuwin Current. The former studies while having greater time and space scales are still not based on a sufficiently large data base to adequately resolve the seasonal signal along the continental slope off Western Australia.

In this report an attempt is made to assemble appropriate data that will provide a picture of the Leeuwin Current throughout the year and which will hopefully shed some light on its origin. Such a data set will need to be able to address the following points. The results of Cresswell and Golding 1980 reveal that the Leeuwin Current is a strongly seasonal phenomenon and also that it flows predominately on the continental slope. Hamon (1965, 1972) observed that the presence of vigorous mesoscale eddies in the region meant that the associated noise level is large enough to completely obscure the seasonal cycle in individual cruise results. This means that our data set must have an intensive coverage in both time and space; particularly close to the shelf and that a rather careful statistical approach to the data analysis needs to be adopted. Finally if we hope to gain any insight into the origin of the current we need to consider the seasonal circulation of the whole region 10-40°S; 105-130°E in order to determine the environment within which the Leeuwin Current is actually imbedded.

Since the largest possible data set needs to be assembled, the raw data file of hydrology stations was supplemented with the large number of XBT temperature casts available in this region. Typically XBT sections begin in relatively shallow water adjacent to the continental slope. Therefore there is a much greater chance that presence of the Leeuwin Current will be evident in the data. The use of TS relations from Ridgway and Loch (1986) enables steric height to be calculated from XBTs, which was then merged with steric heights obtained from hydrology stations. Finally the annual cycle of mean sea level as deduced from coastal tide gauges, was used to extrapolate the steric height topographies onto the continental shelf.

This report presents comprehensive displays of the annual mean and seasonal steric height relative to 1300 db, at surface and subsurface levels. These maps are the first to give an objective description of the average seasonal and spatial distribution of the Current. In Godfrey and Ridgway (1985a) a discussion of the dynamics of the region as inferred from this data is given, which includes both a possible mechanism for the Leeuwin Current and the origin of the unique character of the Western Australian circulation.

2. DATA AND METHODS

The results obtained in this report are based on historical hydrology (Nansen stations) and XBT data held by CSIRO, Division of Oceanography and the Australian Oceanographic Data Centre (AODC) respectively. Both data sets cover a region within 10°-40°S and 105°-130°E, over a period from 1950-80. A further source of data is a set of monthly mean sea levels, at tide gauges around the coast of Western Australia, obtained from Flinders Institute of Atmospheric and Marine Sciences. The location of these stations are given in Fig. 1 - data typically cover a 15 year period, 1966-1980.

Determination of 0/1300 steric height

Steric height, at the surface relative to 450 db is computed from the hydrology data using standard methods (Lafond 1951) and from XBT data using the mean TS relationships given by Ridgway and Loch (1986). Since the 450 db level is too shallow a reference level for study of (for example) the Sverdrup relationship in the region the data are used to obtain steric height to 1300 db. A variant of Hamons (1968) technique is applied to estimated 450/1300 steric height from the XBT casts and shallow (less than 1300 m) hydrology stations.

Hamon found that in the Tasman Sea the geopotential topography can be estimated directly from the near surface temperature structure. Variations of this technique have been used by Nilsson and Cresswell (1981) and Boland and Church (1981) for the Tasman Sea and by Andrews (1976) off Western

Australia. A summary of these techniques, for the former region, is given by Pearce (1983).

In the present application, 450/1300 steric height is obtained as a function of 300/450 steric height: linear regression relationships of the form

$$H_{450/1300} = \alpha + \beta \quad H_{300/450} \qquad (1)$$

(where $H_{x/y}$ is steric height at x relative to y and α and β are regression constant and coefficient) are generated within 5° latitude bands between 10°-35°S. At each station of at least 450 m depth, $H_{0/450}$ computed from observations is added to $H_{450/1300}$ from (1) to give an estimate of $H_{0/1300}$.

Network of bins

The data are divided into the network of bins illustrated in Fig. 1. The arrangement is the end result of a trial and error procedure, and represents a compromise between the resolution of essential features of the circulation and the retention of a statistically reliable number of observations in each bin. The narrow shelf hugging bins, located between 20° and 35°S, have been chosen particularly to follow the known spatial extent of the Leeuwin Current. Unfortunately, lack of data has prevented the use of similar bins along the South coast of Australia, and north of 20°S.

The upper number in each bin represents the total number of stations and the lower number in each 5° band is the number of 1300 m stations within that band.

Corrections for spatial distribution of data

Since all data within a bin are to be averaged such that an effective steric height value is obtained at the midpoint of the bin, a correction procedure is applied to allow for variations in spatial distribution of the original stations. Hamon (1965) showed that the mean steric height drops 0.55 m between 15° and 32°S. This steady decrease is also evident in the 0/1000 db geopotential anomaly maps of Wyrtki (1971). Therefore the data are corrected for latitudinal variations from the midpoint of each bin (between 15° and 30°S) using the slope of this linear variation. Corrections to individual data points are sometimes as large as 0.07 m, but corrections to seasonal mean curves are seldom greater than 0.02 m presumably because cancellation of these departures occurs.

No allowance has been made for the more irregular and rapid zonal changes in steric sea level, since unrealistic "corrections" might have resulted near the edges of the study region.

Seasonal best-fit curves

We assume initially that the result $h(n)$ of any steric sea level measurement on day t_n in a particular bin takes the form

$$h_n(t_n) = A_0 + \sum_{j=1}^{4} A_j X_j(t_n) + R_n = H(t_n) + R_n, \tag{2}$$

where $X_1 = \cos(2\pi t/T)$, $X_2 = \sin(2\pi t/T$, $X_3 = \cos(4\pi t/T)$, $X_4 = \sin(4\pi t/T)$, $\sin(4\pi t/T)$ $T = 365.25$ days and R_n is a Gaussian-distributed independent random number with zero mean and standard deviation σ; and $H(t)$ is the 'true' seasonal signal we are trying to estimate (assumed here to contain only annual and semiannual terms).

If a finite number N of observations is taken, a least-squares best-fit curve

$$h(t) = a_0 + \sum_{j=1}^{4} a_j X_j(t) = \bar{h} + \sum_{j=1}^{4} a_j x_j(t) \tag{3}$$

can be obtained by multiple linear regression in the variables X_1, X_2, X_3, X_4 (e.g. Snedecor and Cochran, 1967; Bennett and Franklin, 1954).

In (3), a bar denotes an average over the observations; $x_j = X_j - \bar{X}_j$; and

$$a_j = \sum_{j} C_{ij} q_j, \tag{4}$$

where C is the inverse of the matrix whose elements are

$$\sum_{n=1}^{N} X_{in} X_{jn}, \text{ and } q_i = \sum_{n=1}^{N} X_{in}(h_n - \bar{h}).$$

We need to find an rms magnitude of the departure of $h(t)$ from $H(t)$, throughout the year.

This is difficult for two reasons. The first is that steric height data are often unevenly distributed, with gaps at certain times of the year.

A more serious problem, however, lies in the fact that the non-seasonal departures of the steric height from the 'true' seasonal cycle are correlated with one another because of mesoscale eddy effects and large-scale interannual variations.

In Godfrey and Ridgway (1985b) both of these problems are considered and they show that $E(t)$, the standard error in the estimate of the seasonal cycle, may be itself estimated by the expression

$$E^2(t) = Q\,\sigma^2 \left[\frac{1}{N} + \sum_{i=1}^{4} \sum_{j=1}^{4} C_{ij}\, X_i\,(t)\, X_j(t) \right] \qquad (5)$$

where Q represents the effect of the correlation of non-seasonal departures. Q is actually a function of time and of the distribution of observation times $t_1, t_2, \ldots . t_N$. However, Godfrey and Ridgway approximate it by a constant $\bar{Q}$, and assume that $\bar{Q}$ has the same value in all bins. The effective number of degrees of freedom in a bin is then $N/\bar{Q}$.

In this report following Godfrey and Ridgway (1985a) a value of 1.71 is used for $\bar{Q}$.

A choice of equivalent mean steric sea level for coastal tide gauges

As a means of displaying both the annual mean and seasonal geostrophic flow, contours of steric height at the surface for the whole region between 10°-40°S and 105°-130°S are obtained from the 2 harmonic best fit curves given in (3).

The contours have been extrapolated into the coast assuming that the rate of change of sea level with distance offshore is the same over the shelf as it is between the first and second offshore bin of steric sea level. Longshore currents along a straight continental shelf are generally in accurate geostrophic balance across the shelf, so this method of extrapolation into the coast implies an assumption that annual average longshore currents over the shelf are the same as they are between the first and second offshore steric sea level bins. Although this is not necessarily true, by making this assumption we are able to ascribe an annual average "equivalent steric sea level" at each tide gauge site. When tides are removed from the raw tide gauge record, the inverse barometer effect corrected for, and a constant added to the result, such that the annual mean of the record equals the value assigned to it, we can treat the result as an "equivalent steric sea level" for the tide gauge. This procedure permits us to include monthly mean sea level values from coastal tide gauges on seasonal maps of steric sea level; however it must be borne in mind that the resulting maps show only an assumed annual average longshore current over the continental shelf. Provided this limitation is remembered, seasonal maps of sea level extending into the coast can be obtained. They are useful tools for studying circulation patterns in the Western Australian region.

It may be noted that we have not attemped to fit the coastal sea level data with a two-harmonic best fit, but have simply used the mean sea level for each month of the year; thus geostrophic current estimates may contain higher harmonics.

3. RESULTS

Regression of $H_{450/1300}$ with $H_{300/450}$

The linear regression relationships in Table 1 were obtained within 5° latitude bands between 10° - 35°S, from the hydrology data set.

The regression curve for 10°-15°S is plotted in Fig. 2(a) along with the raw data.

South of Australia, in the waters between 105° and 130°E, the method broke down and no regression relationships could be obtained. Figure 2(b) shows that whereas a negligible variation in $H_{300/450}$ exists, $H_{450/1300}$ ranges from 0.75 to 0.98 m. To obtain an estimate of $H_{0/1300}$ in these bins the mean value of $H_{450/1300}$ was added to each $H_{0/450}$ observation.

As a check of the estimation technique, 0/1300 steric heights obtained (H) from the conventional method at the deep stations, were compared with the values (H') obtained from the above regression relations. It was found that RMS differences in each 5° band were in the range 0.01 to 0.05 m and that 80% of the differences, $H-H'$, were less than 0.05 m. This is in the range of the inherent error associated with a calculation of steric height given by Emery (1975). Even in the bins to the south, between 35°-40°S (S,T,U), where a mean $H_{450/1300}$ value was used, RMS differences of order 0.04 m were obtained. Frequency histograms of the magnitude of the differences between estimated and true dynamic heights for each 5° latitude band are displayed in Fig. 3.

Seasonal best-fit curves

The seasonal best-fit curves computed in each bin are presented in Figs 5(a)-(u), along with the $H_{0/1300}$ steric height observations on which they are based. The error bars represent the RMS deviation from the 'true' curve, derived from the procedures described earlier. The RMS values tend to be larger at times of year when data are sparse, as expected; the majority of RMS values are less than 0.05 m.

Overall the scatter of observations underlines the large variability in steric height as reported by Hamon (1965) and the corresponding difficulty in obtaining a seasonal signal from the background noise. Within each bin, the range of individual steric height values lies between about 0.35 m to as high as 0.8 m.

The seasonal curves are considered from north to south in Fig. 5, employing the bin nomenclature given in Fig. 1, where Fig. 5(a) corresponds to bin A, Fig. 5(b) to bin B etc.

Between 10°-15°S (Fig. 5(a)) curve A shows little seasonal variation while curve B has a distinct biharmonic character. The large size of bins and

the frequent data gaps contribute to the rather large RMS values, so care must be expressed in making definite conclusions. At the western edge of the region there are relatively many observations, so we have split the 10°-15°S band into two (regions *C* and *D*, Fig. 1) to resolve the west flowing South Equatorial Current: this current is revealed by steric height differences between bins *C* and *D* which range from 0.23 to 0.05 m. The increase in steric height in *C* between March and September (and corresponding decreases in steric height difference between the bins) is associated with the previously observed northward migration of the South Equatorial Current (Wyrtki 1961; Hamon 1965).

Further to the south, between 15° and 20°S (Figs 5(e),(f),(g)), the three curves display minimal seasonal variation. Curve *F* is lacking in data, particularly in summer which means that the RMS values are large, however, curve *G* possesses a much greater number of observations spread uniformly throughout the year.

Perhaps the most prominent seasonal change in steric height, as indicated by the best-fit curves, is given in Fig. 5(h) within bin H (between 20°-25°S). A rise of 0.27 m occurs in the period, February to May. This corresponds to a rapid build up of sea level which ultimately appears to drive the poleward flowing Leeuwin Current (Godfrey and Ridgway, 1985a). Both the background scatter of data and the magnitude of RMS deviations leaves no doubt that this rise is a real phenomenon. In contrast, the small annual variation in the adjacent bin (*I*) suggests that the rise is trapped relatively close to the coast. The second maximum in regions I occurring in September, appears in sharp contrast to the patterns of steric height observed in the adjoining bins - in both of these the curves remain approximately constant from August to December. However when seasonal steric heights from those curves are used to produce relief maps in the next section, this particular curve is not inconsistent with the overall patterns.

Steric height differences between the two nearshore bins (*H* and *I*) suggest the presence of southward geostrophic currents in May-July and northward flow in the September-November period.

Moving further southwards, Figs 5(k) to (q), a maximum in the steric height curves is observed in autumn and winter, particularly in the inner shelf bins (*K* and *O*), but also to a lesser extent further offshore (*L,M* and *P,Q*). This maximum corresponds to the seasonal appearance of the Leeuwin Current. A much clearer picture of the seasonal development of the Leeuwin Current is seen in the steric height maps for the whole region as discussed later.

Unfortunately gaps exist in the data in certain strategic periods (e.g. June-July in bin *K*) which means that confidence limits are increased. This emphasizes the necessity of further data collection before the seasonal cycle can be accurately resolved.

The bins south of Australia (*S,T,U*), Figs 5(s),(t),(u), show much reduced steric heights with annual means of order 1.6 m. The 3 curves have similar seasonal patterns with broad maxima centred in May and minima in spring. The range of steric height is however only about 0.07 m. Unfortunately the data coverage in this region is poor - certainly below that needed to resolve any circulation features near the continental shelf.

Annual mean steric topography

Annual means of steric height of the surface relative to 1300 db obtained from the two harmonic steric height curves are presented in Figs 6(a) and (b). The two maps only differ in the choice of extrapolation procedure of the isoteres into the coast (indicated by the dashed lines over the continental shelf). In Fig. 6(a) the contours are drawn assuming the longshore gradient of geostrophic current between the coast and the first offshore bin is the same as between the first and second offshore bins. The extrapolations in Fig. 6(b) are adjusted to allow for the possibility that some of the annual mean flow from the Pacific to the Indian Ocean (Godfrey and Golding 1981) may occur along the continental shelf between Irian Jaya and Australia.

The overall pattern is quite smooth in the offshore region; the major feature is the increase of steric sea level from south to north, as already mentioned. This drives the broad scale eastward geostrophic flow into the W.A. coast which is observed between 15°-32°S. As the continental shelf is approached, this inflow turns southeastward, and is accelerated parallel to the shelf to the vicinity of Cape Naturaliste; here a major component of the flow pivots eastward and continues along the south coast of Australia.

Figures 7(a), (b), (c) and 8(a), (b) show the annual means of steric height at the 100, 200, 300, 450 and 700 db surfaces, relative to 1300 db. The first three are obtained by averaging monthly values of the two harmonic curves (i.e. in a similar manner to the surface steric heights in Fig. 6). The latter 2 figures (at 450 and 700 db) are based on the Nansen bottle data (for stations reaching 1300 m).

The pattern at 100 db in Fig. 7(a) is very similar to that at the surface with generally southeastward flow between 28.5°-35.5°S. In Fig. 7(b) poleward geostrophic currents are evident along the continental shelf down to 200 m between NW Cape and Cape Naturaliste but are no longer evident at the 300 db surface (Fig. 7(c)). At the 450 and 700 db levels a northward undercurrent is present, and also longshore steric height gradients of 8 and 5 cm respectively; Thompson (1984) suggests that the pressure gradient drives the northward undercurrent.

Figure 7(c) also shows that at this surface some southeastward inflow remains (between 30-35°S) but that there exists a band of westward outflow further north from 20-25°S. No eastward flow around Cape Leeuwin is possible at the 200 and 300 m depths as strong negative steric height gradients are present.

Seasonal steric height anomalies

At the surface, maps of the seasonal steric height anomalies are presented at 2 monthly intervals in Fig. 9. The seasonal cycle is discussed in detail in Godfrey and Ridgway (1985a) so only a brief description is given here.

As a means of illustrating the anticlockwise progression around the coast, regions of positive anomaly are shaded. If one ignores the pattern in the north-west corner (related to the South Equatorial Current) the rather irregular passage of this 'wave' can be seen: entering from the northeast in January, moving both southward and westward in March and May and then progressively being overtaken by the negative anomaly in July to November. The strongest currents both poleward and equatorward are located just near and on the continental shelf.

The patterns of seasonal anomalies at the surface and at 100, 200 and 300 db exhibit strong similarity throughout the year. This occurs despite the fact that surface contours use coastal seasonal observations which are not available of course at the subsurface layers. For brevity only the patterns at the surface and 300 db (Fig. 10) are included. As it happens the anomalies at these two surfaces show the highest correlation. The amplitude of the 'wave' at each surface is 0.15, 0.11, 0.07 and 0.04 m respectively.

It is interesting to observe that the seasonal signal penetrates to a depth of 300 m and almost certainly deeper while the annual mean signal is confined to the surface layer, 0-200 m.

Seasonal geostrophic flow at various surfaces

Surface

The total seasonal steric topography (i.e. mean plus seasonal anomaly) are presented (Figs 11 and 12) with the two choices of geostrophic flow on the continental shelf given in Figs 6(a) and 6(b). The steric relief offshore from the 200 m isopleth are identical in both sets of maps and so they will be discussed together. The hatched regions represent locations with RMS deviations greater than or equal to 0.05 m.

These maps are the first to show an objective coverage of the seasonal and spatial distribution of the Leeuwin Current - the strong poleward-flowing coastal current seen in Fig. 6 to start near North-West Cape and to proceed beyond Cape Leeuwin, in January to July. The inclusion of coastal sea level data is essential for this purpose.

It is convenient to begin the discussion with the July pattern (Fig. 11(d)). At this time, the Leeuwin Current is past its greatest strength; the contours of steric sea level north of Cape Leeuwin show no regions of specially close bunching near the coast, so that steric sea level gradient is relatively even along this section of the coast. There are still appreciable currents, however, south of Fremantle and east of Cape Leeuwin perhaps representing vestiges of the very strong May flow.

From July to September steric sea level drops all along the coast. The effect is particularly marked at the southern end of the region, where (for example) the 1.75 m steric height contour migrates about 1000 km from near Esperance to Fremantle. There is a further large westward migration of the

onshore terminus of the 1.65 m steric height contour from September through to November. However, starting in November, sea levels increase near the coast at the northern end of the region. The effect of these increased sea levels works southward, so that by January an intense offshore gradient of steric sea level develops near North West Cape. Southward geostrophic currents develop near here at this time.

By March the incursion of high sea levels from the north appears to have "pushed" its way past Cape Leeuwin, with the development of an eastward current and increased coastal sea levels there; the currents become particularly strong by May. By July, the Leeuwin Current has passed its maximum strength and the next year's cycle is about to begin.

From July one also observes some northward flow slightly offshore at 27.5°S. This appears as a tongue in the 1.65 isostere. By September this feature is evident from about 30°S to 20°S with a bunching of contours occurring off North West Cape and then in November only a bowing of the 1.85 isostere remains.

The corresponding bimonthly patterns with the alternate choice of coastal means differ slightly on the continental shelf. This may be observed in the respective January-May patterns where Figs 12(a), (b) and (c) shows increased northerly inflow. As stated in Godfrey and Ridgway (1985a) this may in fact be the more realistic situation but further observations of the flow on the Northwest Shelf is needed to make any definite conclusions.

100 db Surface

The circulation at 100 m (Fig. 13) shows a qualitative similarity to that at the surface and hence the seasonal evolution of the Leeuwin Current is clearly evident. Again, beginning discussion of the patterns in July we see that although the southward current is present, the magnitudes have decreased from May. An abrupt transformation then occurs from July to September with northward flow in evidence between 20°-30°S in the latter pattern. A careful examination of the July map does show the beginnings of this at about 28°S just off the shelf. The northward migration of contours appears to stabilize by November and the pattern commences a similar "build up" phase as at the surface and southward longshore currents develop at the shelf break. At this depth the longshore steric height gradient is greatest in May (Fig. 13(c)) and the corresponding steric topography shows strongest flow down this gradient. As an indicator of the above development it is instructive to follow the change over the year, at the shelf break, of the position of the 1.50 m contour.

200 db Surface

At this surface (Fig. 14) steric height gradients are much reduced and the pattern becomes more diffuse and consequently difficult to describe and interpret. The strong system of longshore steric height gradient which exists above this depth between 22°-32°S (and which drives the Leeuwin Current) begins to break down and we see in fact in several months a negative gradient between 22.5° and 27.5°S, e.g. January, March, July and September.

In January and March southward flow is present between 23° and 32°S which must be travelling up the gradient. In Godfrey and Ridgway (1985a) it is postulated that this is maintained by the downwards diffusion of momentum by friction from the upper layer. The strong May flow is still present and at this time the Northwest Cape-Geraldton gradient becomes positive.

Another significant change at this depth is the existence of a negative gradient between Fremantle and Albany. This is of order 5-7 cm and at least within the resolution of the present analysis blocks any flow around Cape Leeuwin.

From July to November the picture becomes rather more complicated. The strong southward flow of May weakens in July and a coastal filament of northward current has developed by September.

300 db Surface

The patterns are even more difficult to interpret at 300 db (Fig. 15) than at the upper surface.

A noticeable feature is a band of westward geostrophic flow between 20-25°S (off North West Cape) throughout the year - most strongly in July. Large north-westward gradients of steric height exist around Cape Leeuwin - although the resolution of the data is poor in this region.

The near shore circulation from 20-35°S NW Cape to Cape Leeuwin is variable - the feature occurring in January is obscure and may not be associated with any real phenomonen. Of interest is the small southward flow as indicated by the 1.075 m contour between Geraldton and Fremantle; perhaps a remnant of the Leeuwin Current.

REFERENCES

Andrews, J.C. (1976) The bathythermograph as a tool in gathering synoptic thermohaline data. *Australian Journal of Marine and Freshwater Research* **27**: 405-15.

Andrews, J.C. (1977) Eddy structure and the West Australian Current. *Deep-Sea Research* **24**: 1133-48.

Bennett, C.A. and N.L. Franklin (1959) Statistical Analysis in Chemistry and the Chemical Industry. Wiley Publications in Statistics, 724pp.

Boland, F.M. and Church, J.A. (1981) The East Australian Current, 1978. *Deep-Sea Research* **28**: 937-57.

Colborn, J.G. (1975) The thermal structure of the Indian Ocean. *International Indian Ocean Expedition Oceanographic Monograph No.* 2.

Cresswell, G.R. and Golding, T.J. (1980) Observations of a south-flowing current in the south-eastern Indian Ocean. *Deep-Sea Research* **27A**: 449-66.

Emery, W.J. (1975) Dynamic height from temperature profiles. *Journal of Physical Oceanography* **5**: 369-75.

Gentilli, J. (1972) Thermal anomalies in the eastern Indian Ocean. *Nature (London) Physical Sciences* **238**: 93-5.

Godfrey, J.S. and Ridgway, K.R. (1985a) The large-scale environment of the pole-ward flowing Leeuwin Current, Western Australia: Longshore pressure gradients, wind stresses and geostrophic flow. *Journal of Physical Oceanography* **15**: 481-95.

Godfrey, J.S. and Ridgway, K.R. (1985b) Estimation of errors in seasonal cycles. *Journal of Physical Oceanography* **15**: 1138-42.

Fofonoff, N.I. (1962) Eastern Boundary Currents, pp. 253-75 in *The Sea*, Vol. 1 (ed. M.N. Hill) New York: Wiley.

Hamon, B.V. (1965) Geostrophic currents in the south-eastern Indian Ocean. *Australian Journal of Marine and Freshwater Research* **16**: 255-71.

Hamon, B.V. (1968) Temperature structure in the upper 250 metres in the East Australian Current area. *Australian Journal of Marine and Freshwater Research* **19**: 41-9.

Hamon, B.V. (1972) Geopotential topographies and currents off west Australia, 1965-1969. *CSIRO Division of Fisheries and Oceanography Technical Paper No. 32.*

LaFond, E.C. (1951) Processing Oceanographic Data. U.S. Naval Oceanographic Publication 614, Washington, D.C., pp 114.

Legeckis, R. and Cresswell, G.R. (1981) Satellite observations of sea surface temperature fronts off the coast of western and southern Australia. *Deep-Sea Research* **28A**: 297-306.

Nilsson, C.S. and Cresswell, G.R. (1981) The formation and evolution of East Australian Current warm core eddies. *Progress in Oceanography* **9**: 133-83.

Pearce, A.F. (1983) Estimation of dynamic heights from temperature profiles in the Tasman Sea. *Australian Journal of Marine and Freshwater Research* **36**: 115-9.

Ridgway, K.R. and Loch, R.G. (1986) Mean temperature-salinity relationships in Australian waters and their use in water mass analysis. *Australian Journal of Marine and Freshwater Research* (in press).

Rochford, D.J. (1969) Seasonal interchange of high and low salinity surface waters off South-West Australia. *CSIRO Australia Division of Fisheries and Oceanography Technical Paper No. 29*

Saville-Kent (1897) The naturalist in Australia. London: Chapman and Hall. 388pp.

Snedecor, G.W., and Cochran, W.G. (1967) Statistical Methods. Iowa State University Press 593 pp.

Schott G. (1933) Auftriebwasser on den Australischen Westküsten? Ya und Nein! Annelen der Hydrographie und Maritimen Meteorologie **61**: 225-333. (In German).

Thompson, R.O.R.Y. (1984) Observations of the Leeuwin Current off Western Australia. *Journal of Physical Oceanography* **14**: 623-8.

Wyrtki, K.J. (1962) Geopotential topographies and associated circulation in the south-eastern Indian Ocean. *Australian Journal of Marine and Freshwater Research* **13**: 1-17.

Wyrtki, K.J. (1971) Oceanographic Atlas of the International Indian Ocean Expedition: National Science Foundation NSF-10E-1.

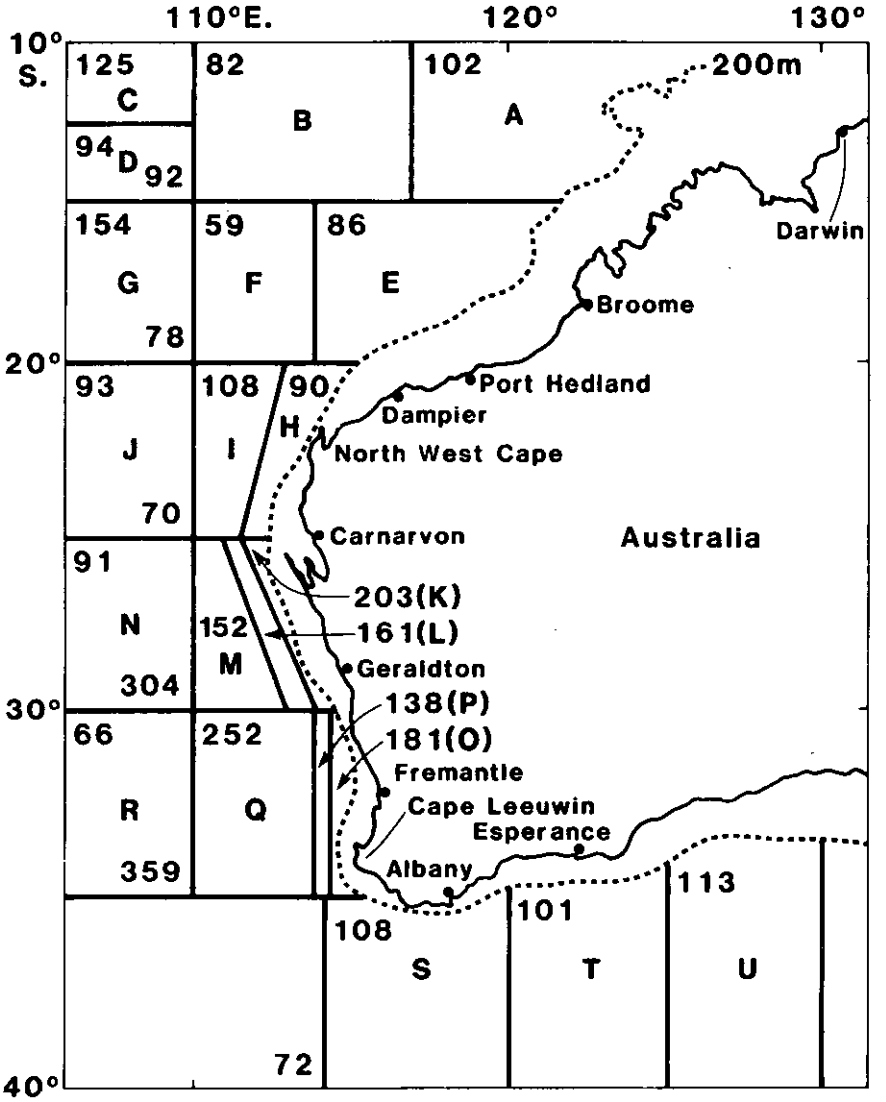

Figure 1 Steric sea level data from hydrographic stations and XBT's were subdivided into the bins shown (A-U). Within each bin, the upper entry is the number of measurements of $H_{0/450}$ within the bin. The bottom number in each 5° band (between 10°-35°s) is the number of observations of $H_{450/1300}$ within the band. The coastal tide gauges are indicated by dots.

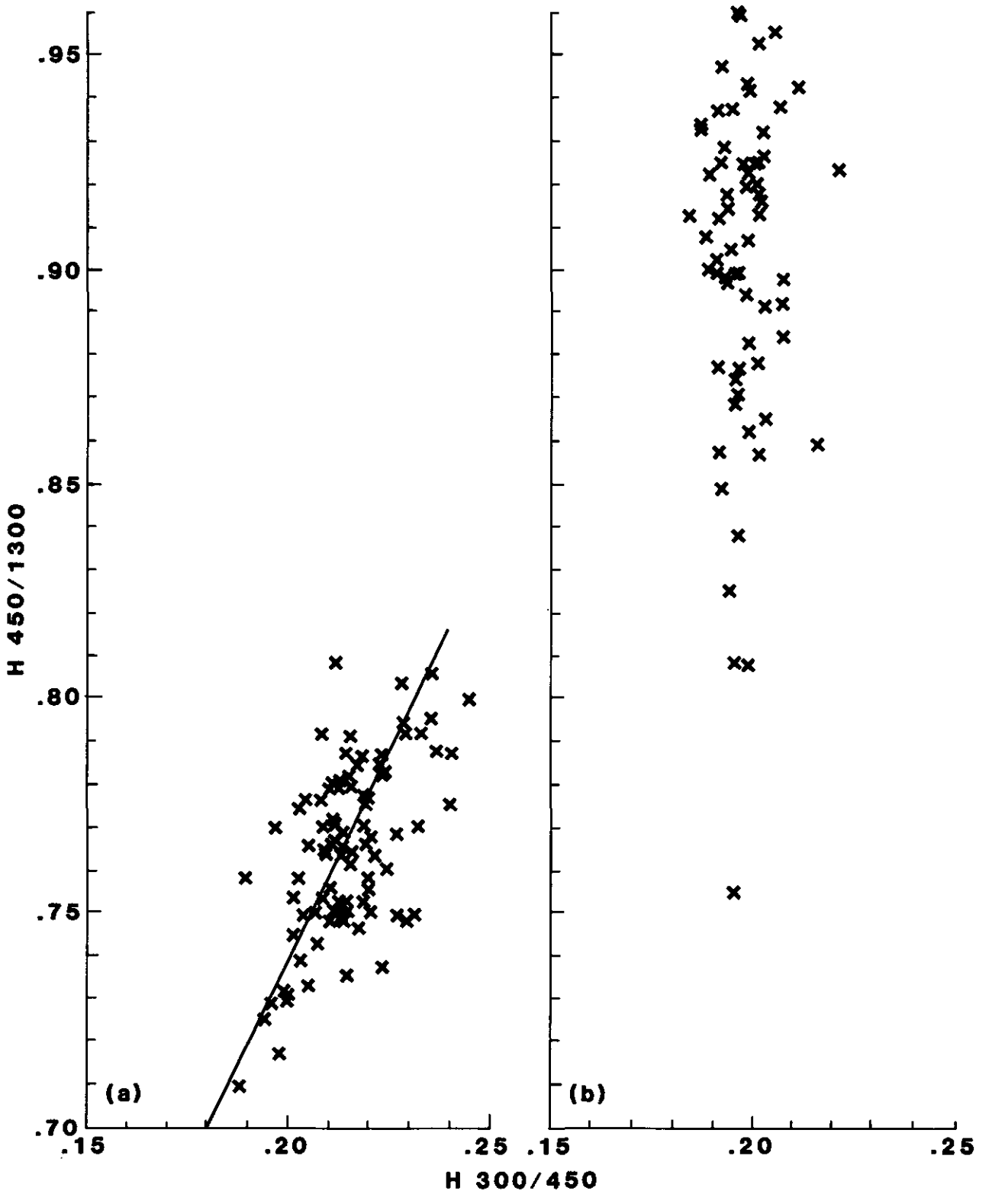

Figure 2a Scatter plot of 450/1300 steric height as a function of 300/450 steric height between 10°-15°S with the derived linear regression curve.

Figure 2b Scatter plot of 450/1300 steric heights as a function of 300/450 steric height within 35°-40°S and 105°-130°E.

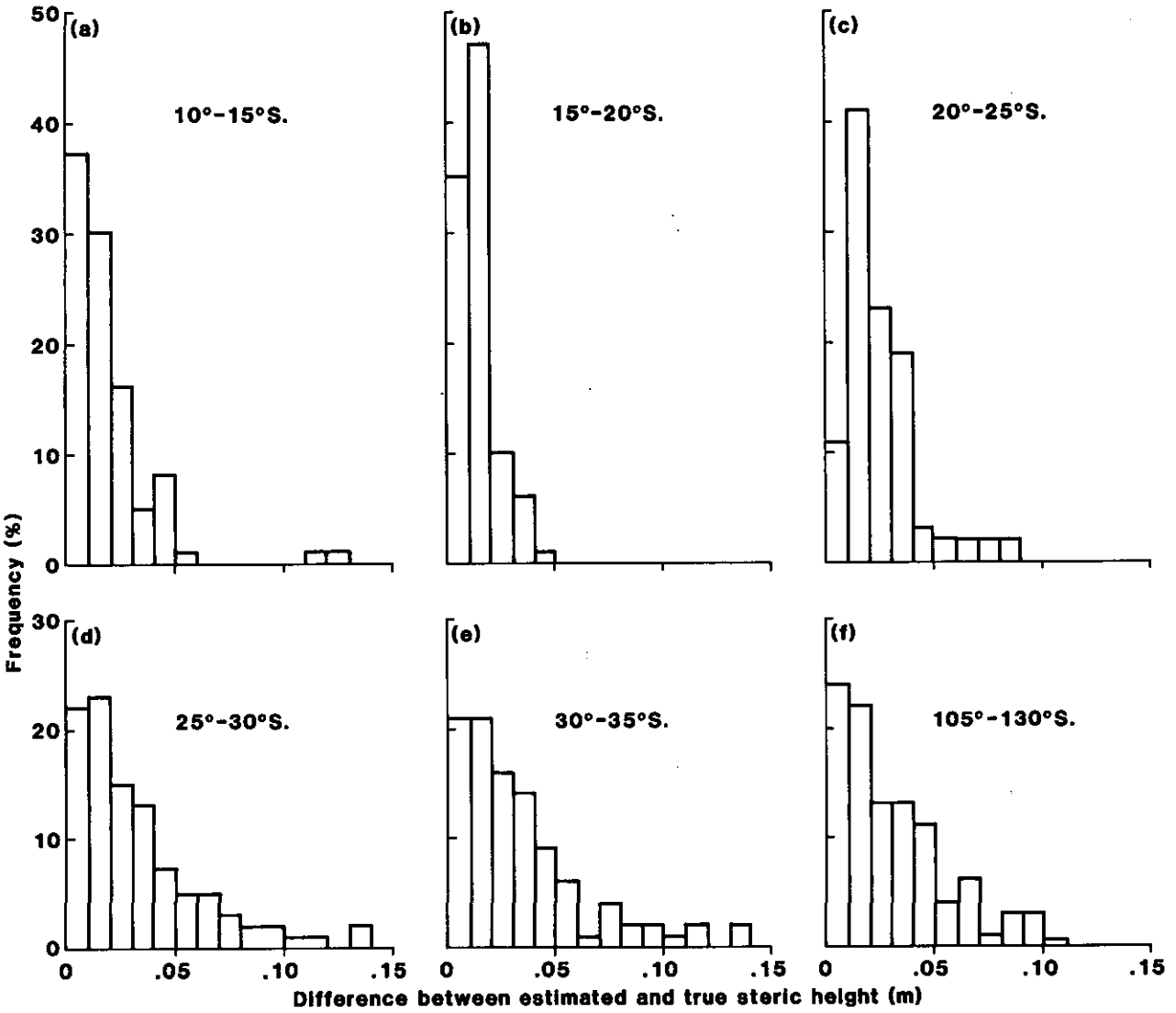

Figure 3 Histograms of the difference between true and estimated steric height for the indicated regions.

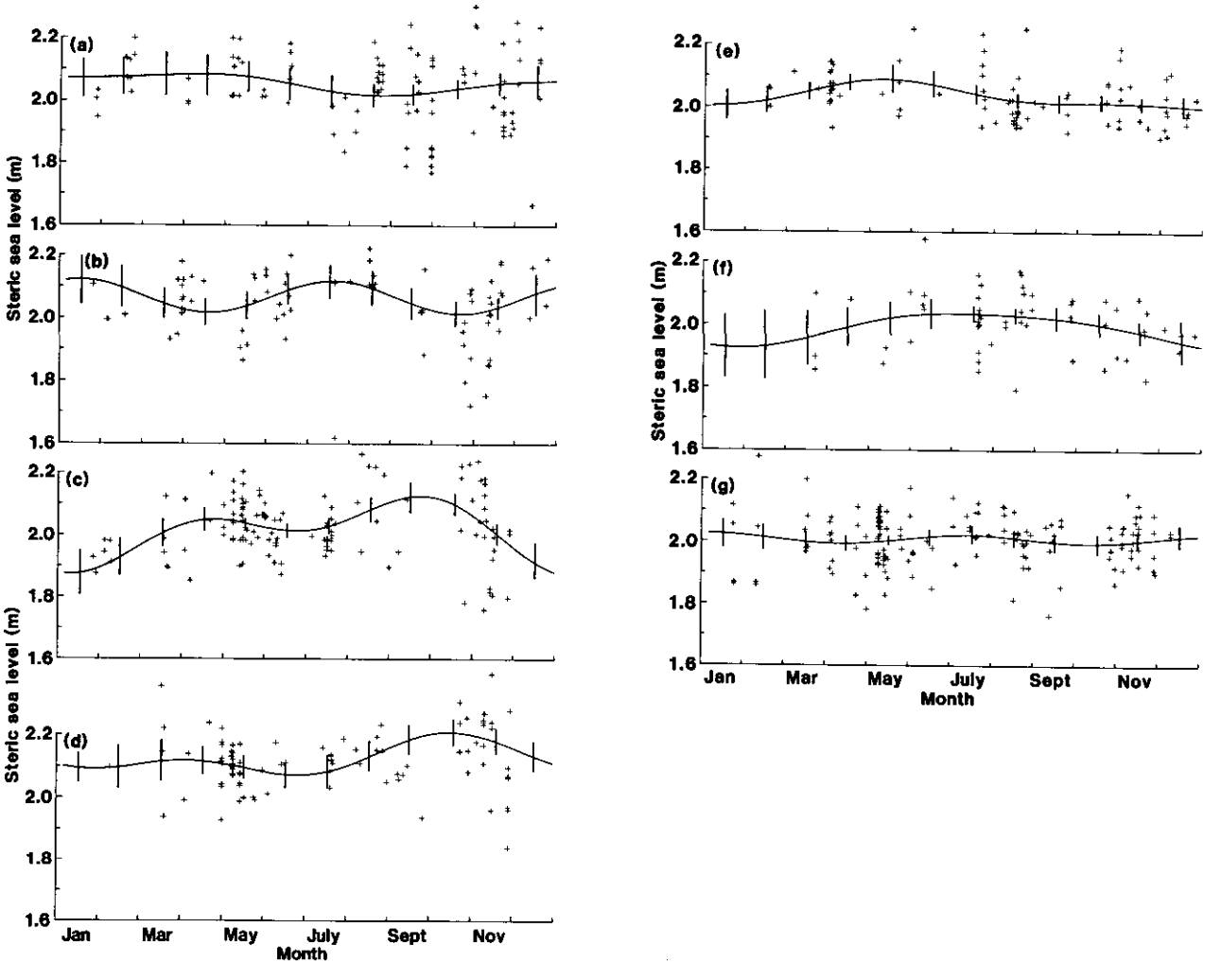

Figures 4a b, c and d Seasonal 2 harmonic best-fit curves of 0/1300 steric height within the 4 bins located between 10°-15°S (A,B,C,D) respectively. The error bars represent RMS deviations from the 'true' seasonal curve and the crosses are the individual steric height observations in each bin. Error bars larger than 0.05 m are in heavy type.

Figures 4e, f and g As for 4(a),(b),(c),(d) except the 3 bins between 15°-20°S (E,F,G).

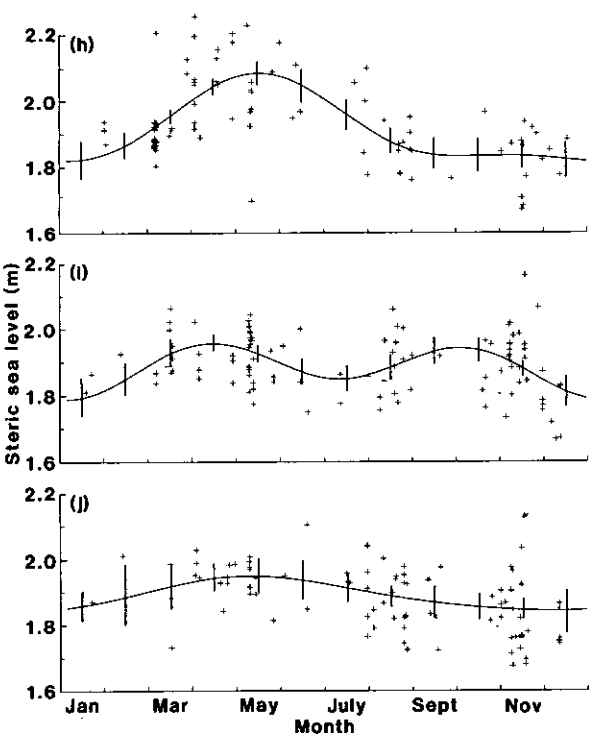

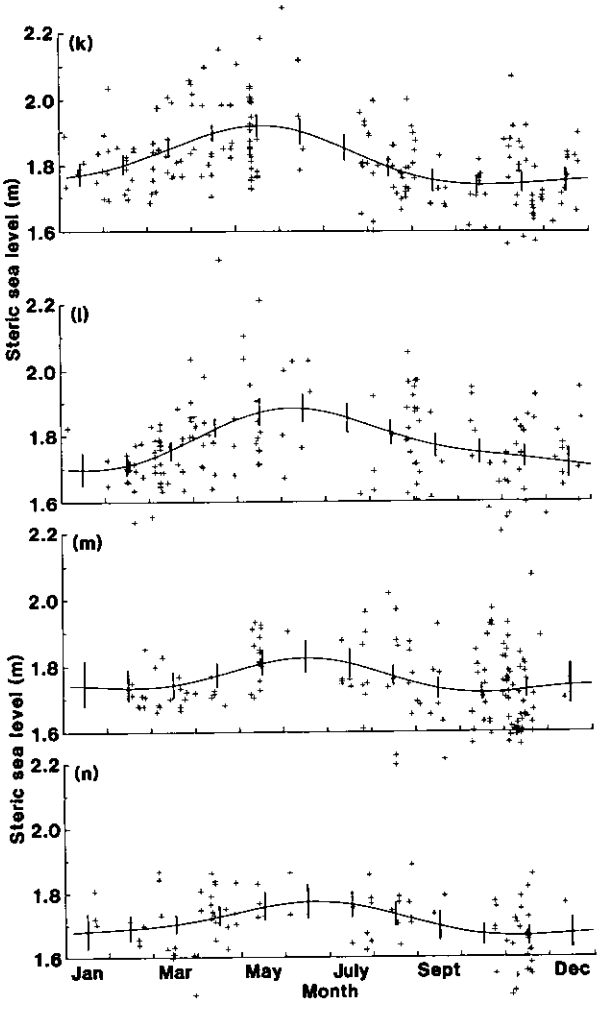

Figures 4h, i, j — As for 4(a),(b),(c),(d) except the 3 bins between 20°-25°S (H,I,J).

Figures 4k, l, m, and n — As for 4(a),(b),(c),(d) except the 4 bins between 25°-30°S (K,L,M,N).

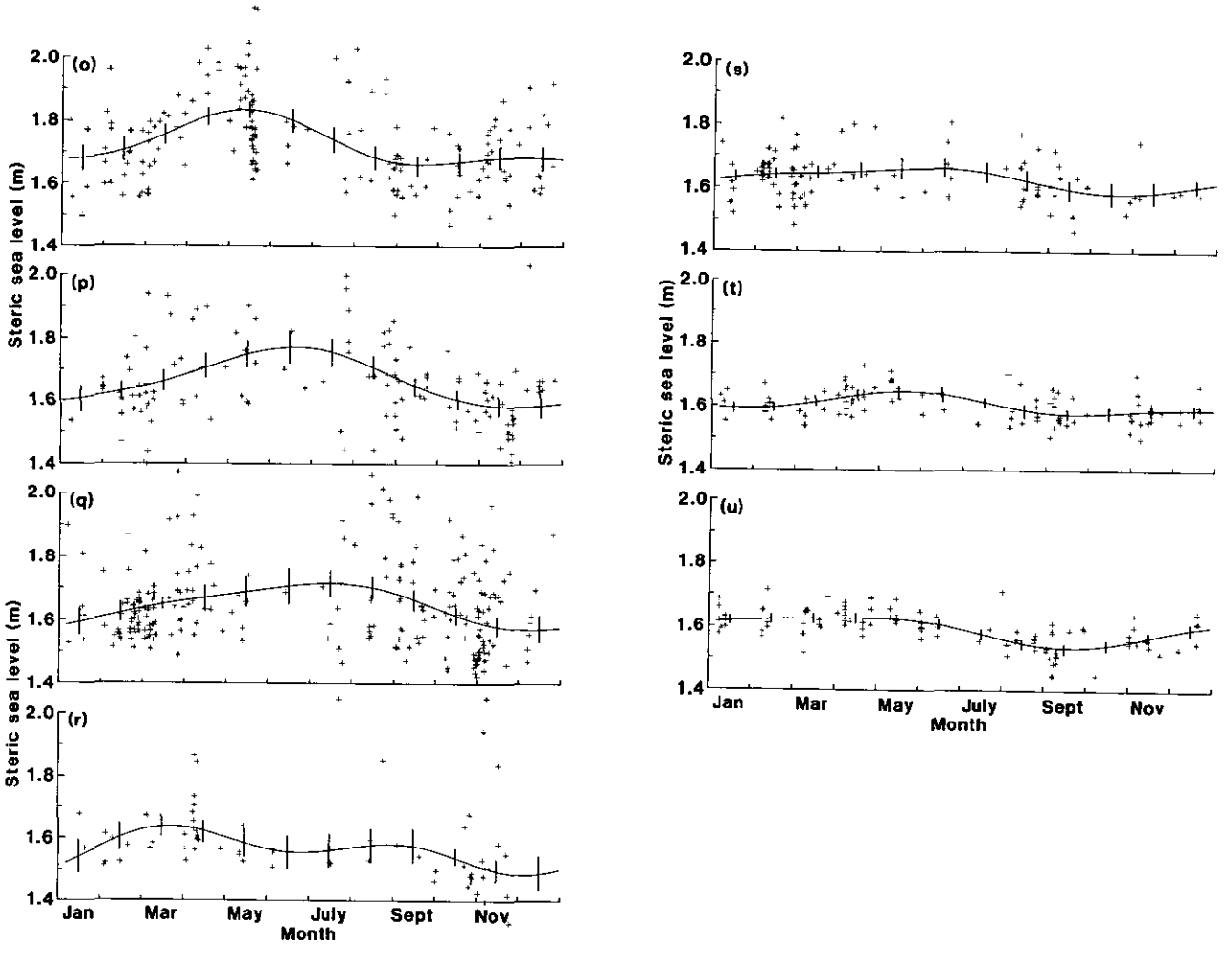

Figures 4o, p, q, and r As for 4(a),(b),(c),(d) except the 4 bins between 30°-35°S (O,P,Q,R).

Figures 4s, t, and u As for 4(a),(b),(c),(d) except the three bins between 114°-130°E and 35°-40°S (S,T,U).

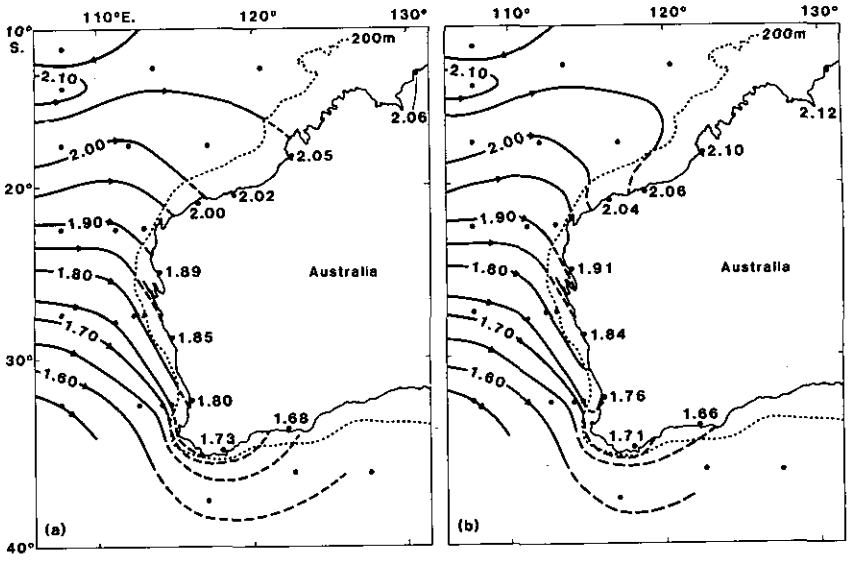

Figure 5a The full lines show contours of annual average steric sea level relative to 1300 db, from the 2-harmonic best fits. The dashed lines are linear extrapolations of these contours into shore. The contour interval is 0.05 m. Figures opposite each tide gauge give the assumed annual mean "steric sea level" at the gauge.

Figure 5b As for Figure 5(a), but with the extrapolation into the coast adjusted to allow for more anticlockwise longshore geostrophic flow from 12.5° to 25°S, and less south of 25°S.

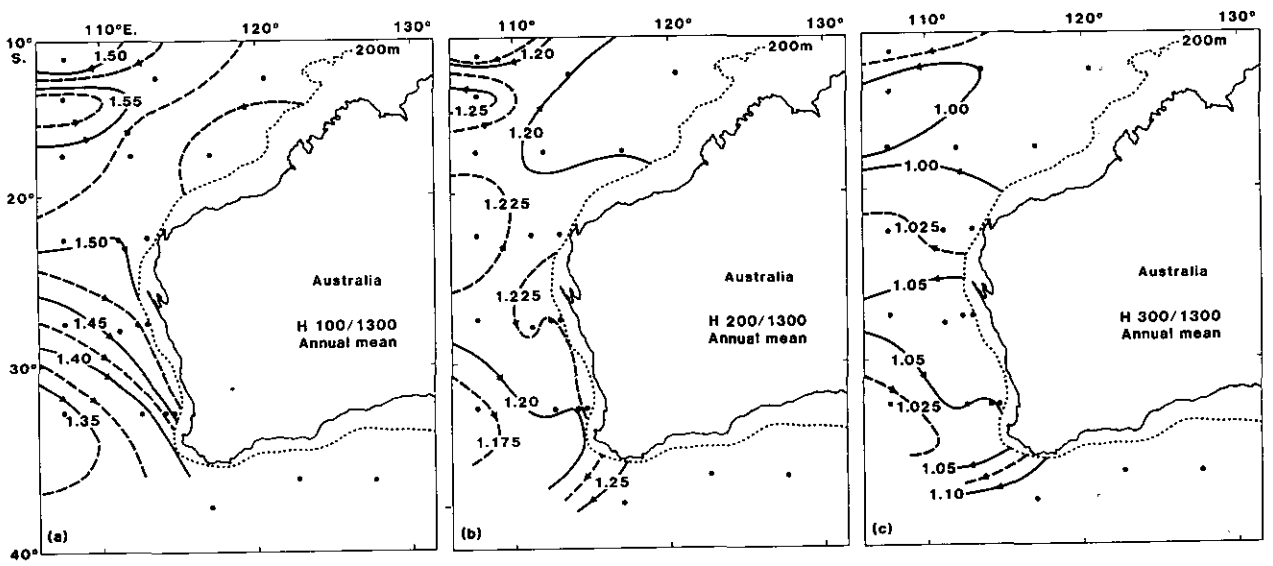

Figures 6a, b and c Annual average steric height relative to 1300 db, at 100 db, 200 db and 300 db obtained in a similar procedure as that at Fig. 5(a). The full and dashed contours are at 0.05 and 0.025 m intervals respectively.

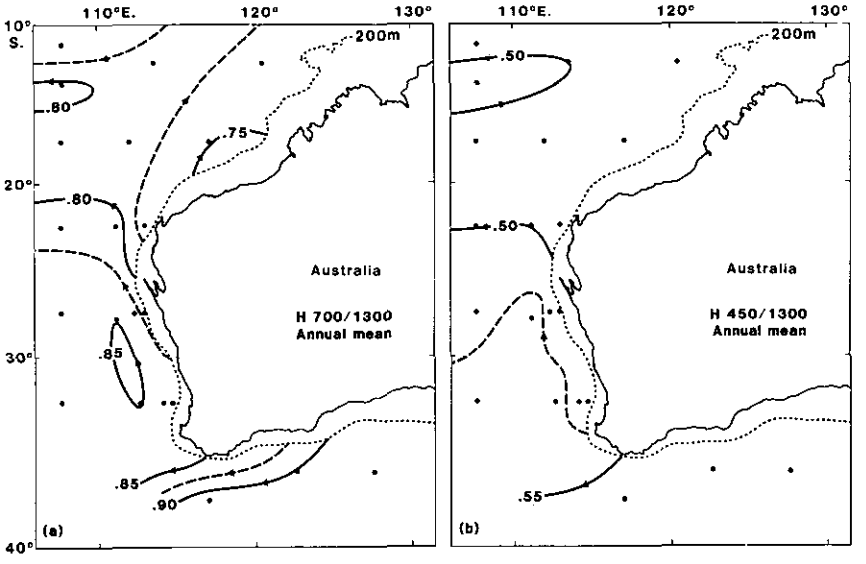

Figure 7a and b Annual average steric height relative to 1300 db at 700 db and 450 db, obtained from Nansen bottle data. The full and dashed contours are at 0.05 and 0.025 m intervals respectively.

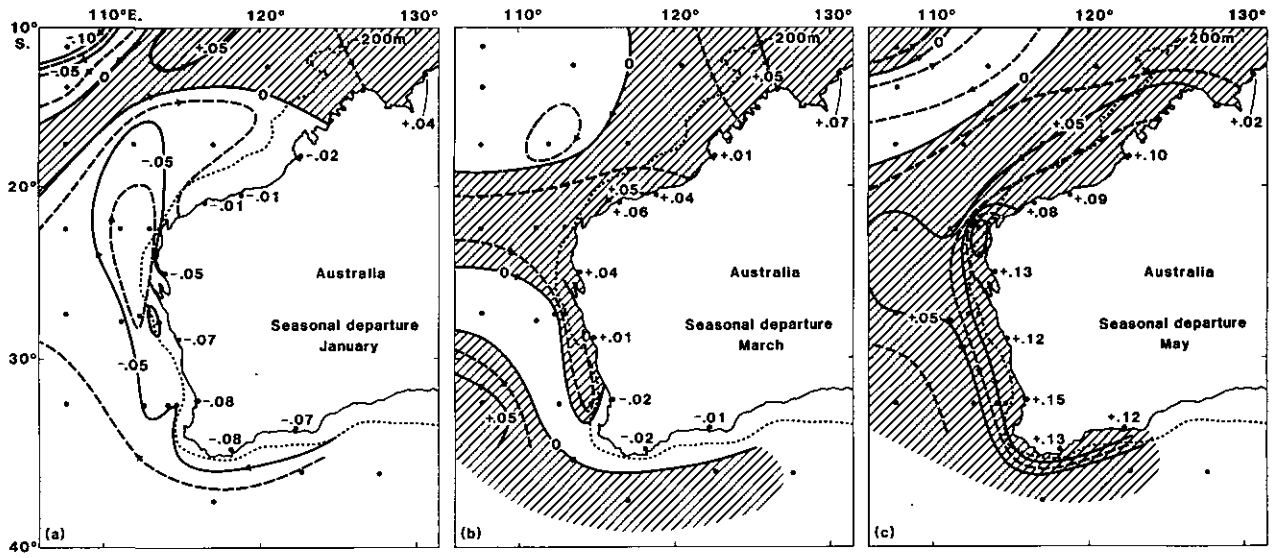

Figure 8a January departures from the annual mean of the two-harmonic best fit to steric sea level, relative to 1300db. Barometrically corrected data from coastal tide gauges have been included; the values are shown, in meters. Stippled areas indicate regions whose r.m.s. deviation from the "true seasonal cycle exceeds 0.05 m. The full and dashed contours are at 0.05 and 0.025 m intervals respectively.

Figure 8b As for Figure 8(a), in March.

Figure 8c As for Figure 8(a), in May.

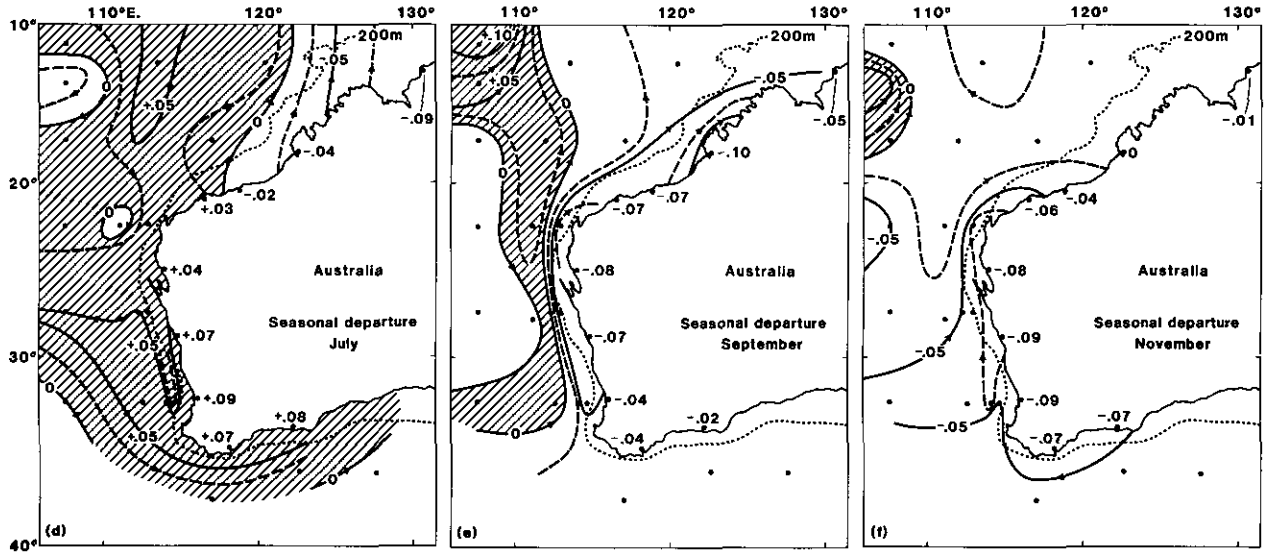

Figure 8d As for Figure 8(a), in July.

Figure 8e As for Figure 8(a), in September.

Figure 8f As for Figure 8(a), in November.

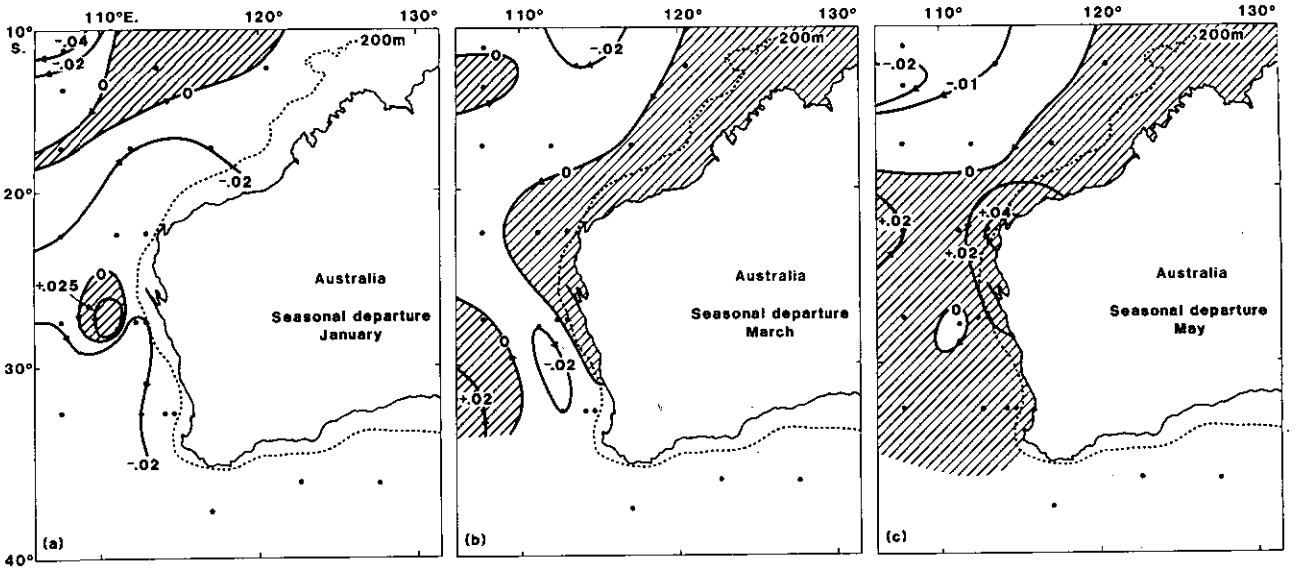

Figure 9a January departures from the annual mean of the two harmonic best fit data to 300/1300 steric sea level. The contour interval is 0.02 m.

Figure 9b As for Figure 9(a), in March.

Figure 9c As for Figure 9(a), in May.

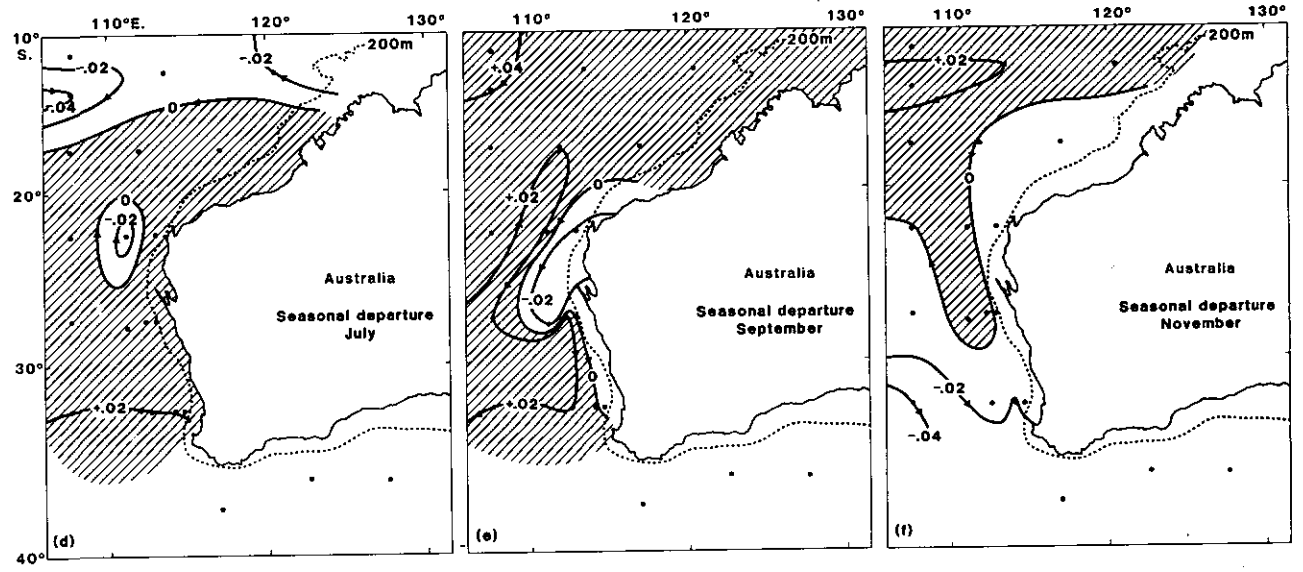

Figure 9d As for Figure 9(a), in July.

Figure 9e As for Figure 9(a), in September.

Figure 9f As for Figure 9(a), in November.

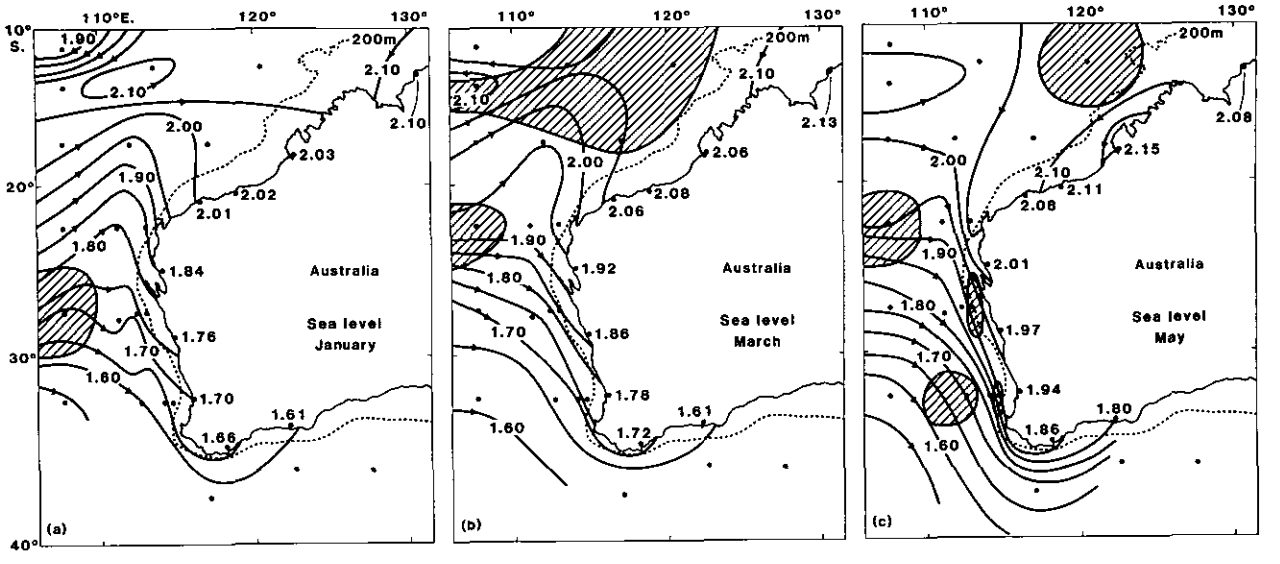

Figure 10a January mean sea level, obtained as the sum of Figure 5(a) and Figure 8(a). The contour intervals is 0.05 m.

Figure 10b March mean sea level, obtained as the sum of Figure 5(a) and Figure 8(b).

Figure 10c May mean sea level, obtained as the sum of Figure 5(a) and Figure 8(c).

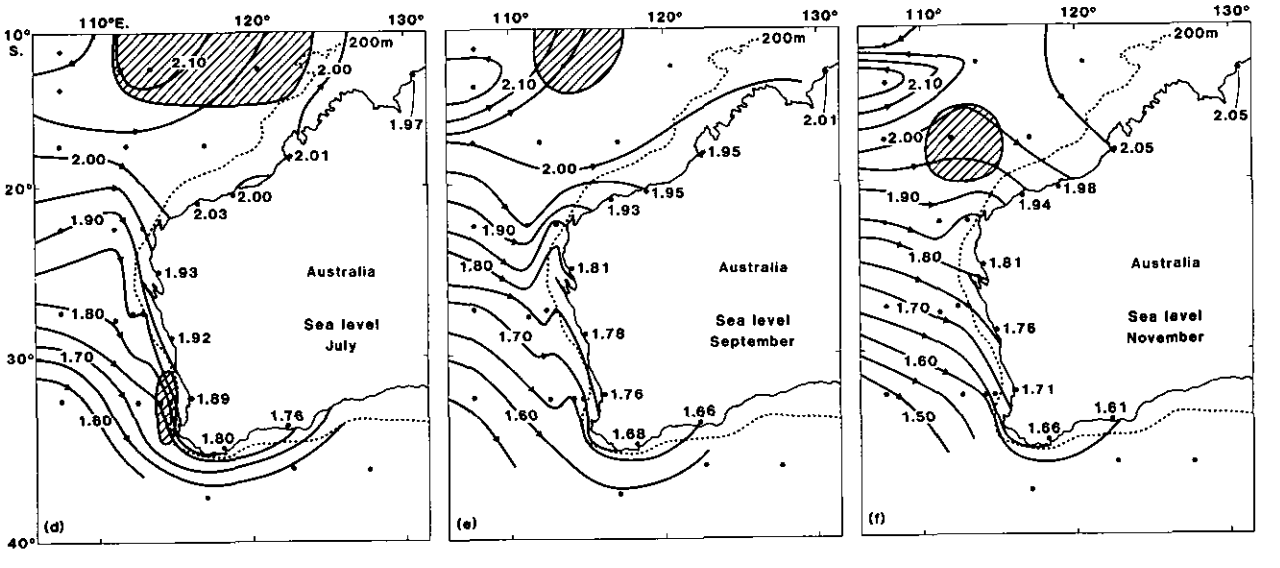

Figure 10d July mean sea level, obtained as the sum of Figure 5(a) and Figure 8(d).

Figure 10e September mean sea level, obtained as the sum of Figure 5(a) and Figure 8(e).

Figure 10f November mean sea level, obtained as the sum of Figure 5(a) and Figure 8(f).

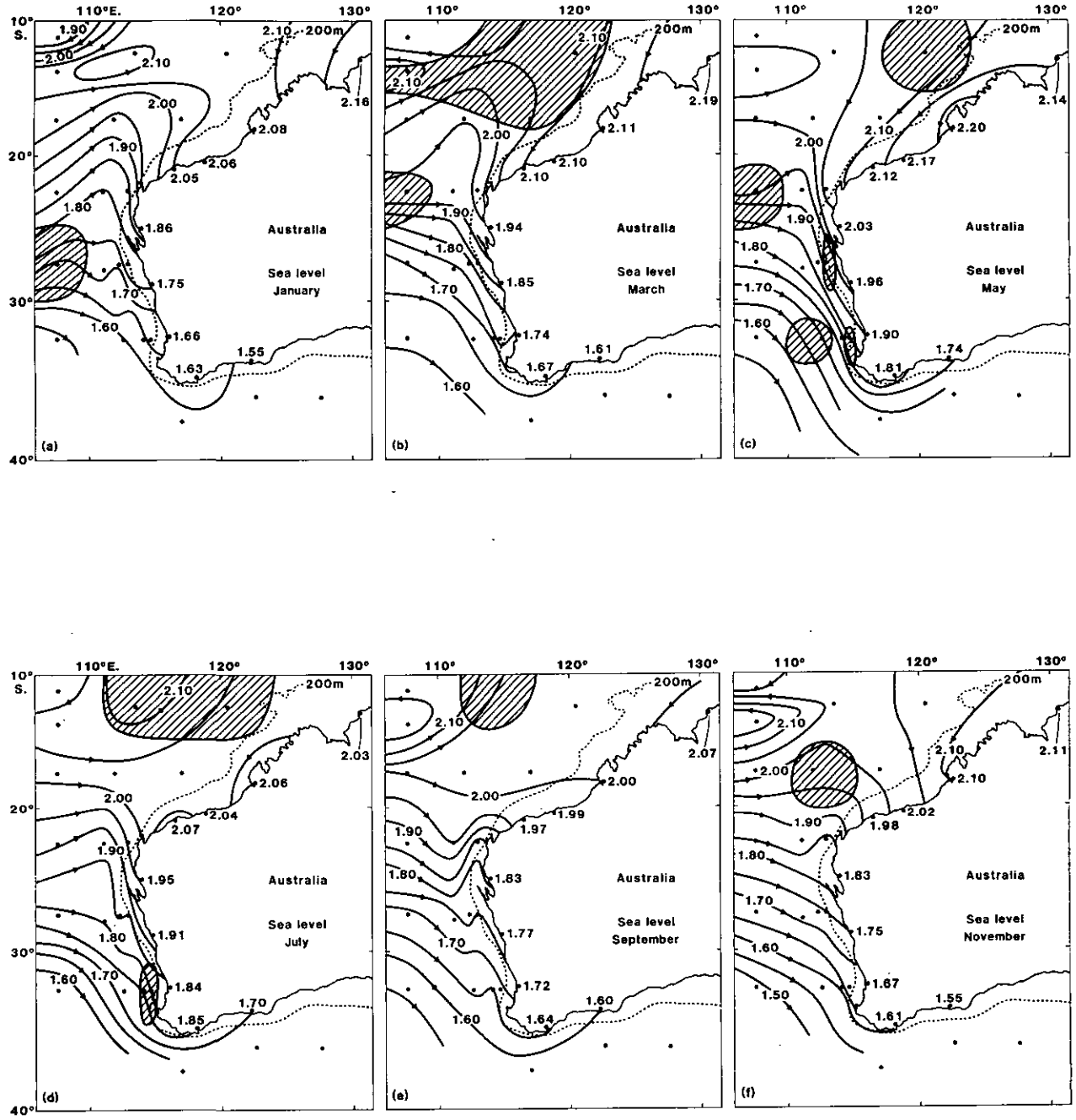

Figure 11 As for Figure 10, but using Figure 6(b) for the annual mean sea level instead of Figure 6(a).

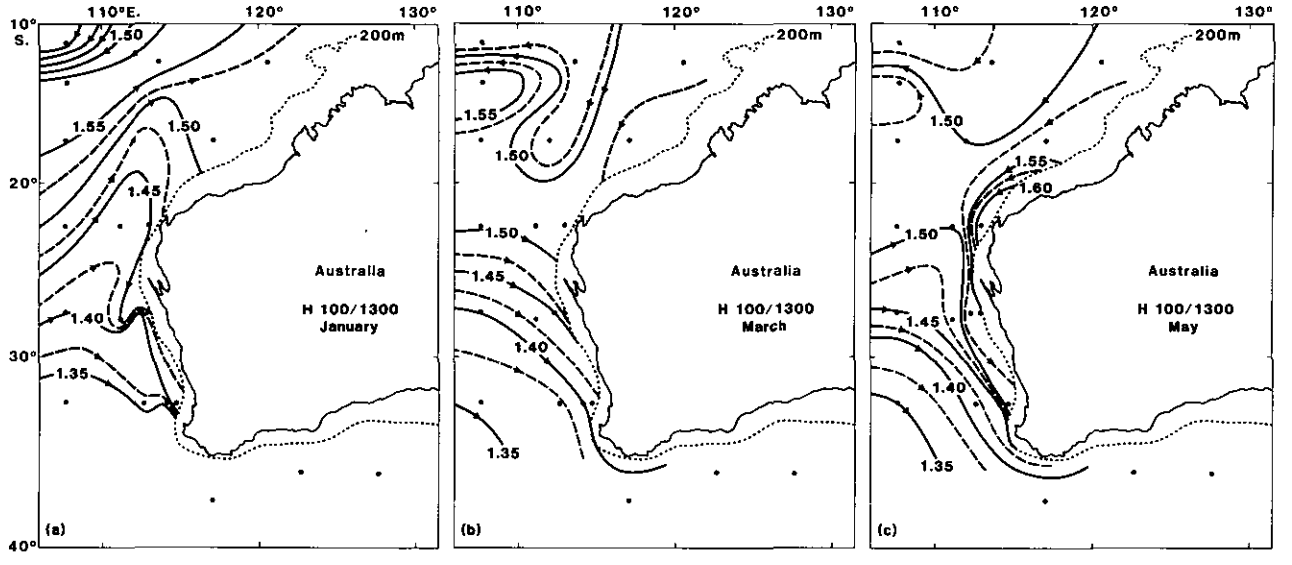

Figure 12a January mean steric sea level at 100 db, relative to 1300 db. The full and dashed contours are at 0.05 and 0.025 m intervals respectively.

Figure 12b As for Figure 12(a), in March.

Figure 12c As for Figure 12(a), in May.

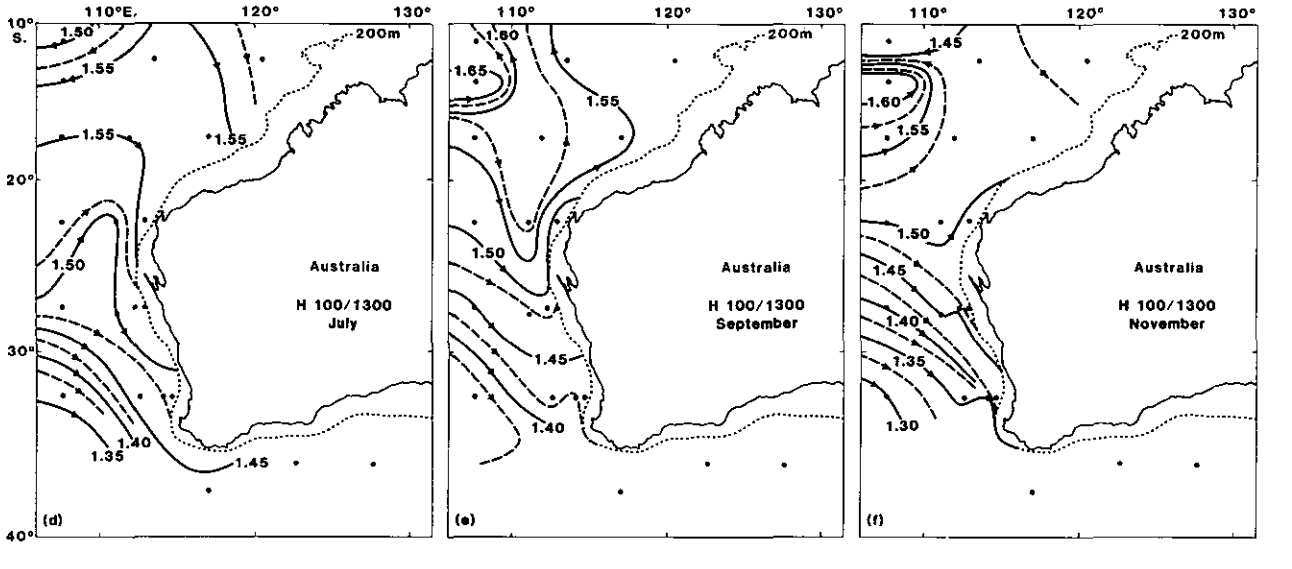

Figure 12d As for Figure 12(a), in July.

Figure 12e As for Figure 12(a), in September.

Figure 12f As for Figure 12(a), in November.

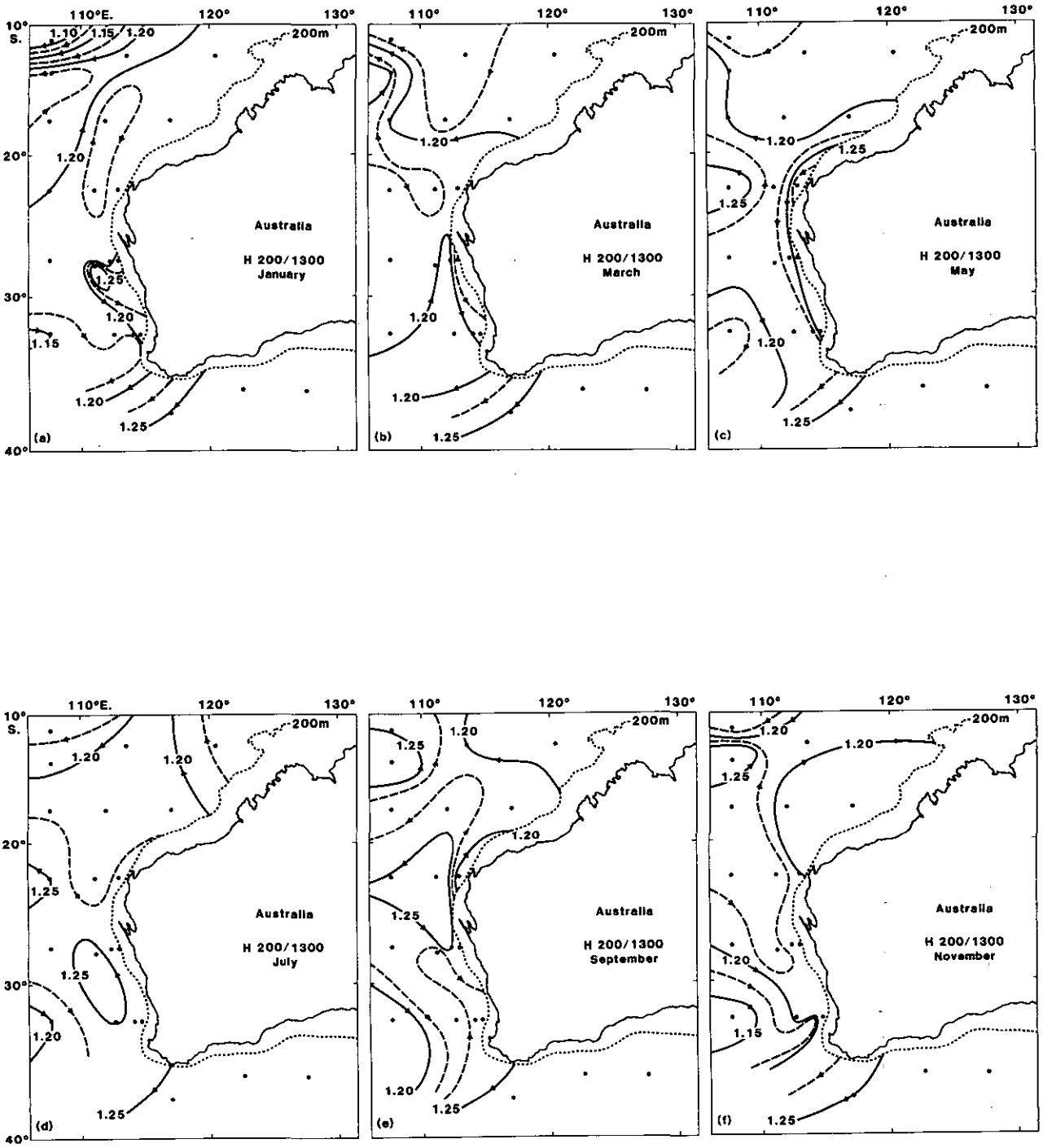

Figure 13 As for Figure 12 at the 200 db surface.

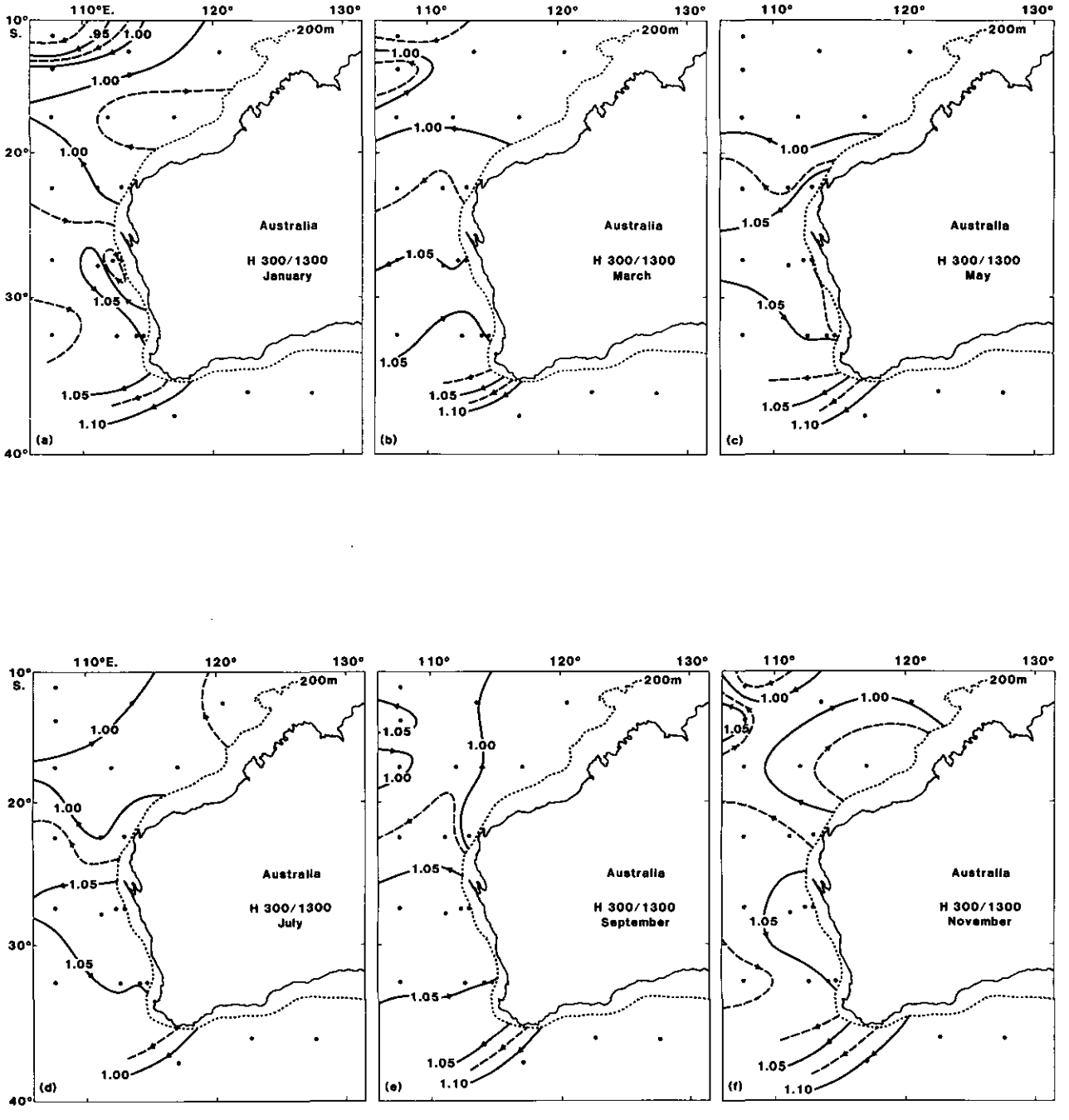

Figure 14 As for Figure 12 at the 300 db surface.

Table 1 Linear relationships of the form $H_{450/1300} = \alpha H_{300/450} + \beta$ obtained in the indicated latitude bands off Western Australia ($H_{450/1300}$ and $H_{300/450}$ are in m).

Latitude Band	α	β	Correlation Coefficient
10 - 15°S	1.9780	0.3437	0.80
15 - 20°S	1.2118	0.4989	0.61
20 - 25°S	1.5465	0.4505	0.53
25 - 30°S	2.2130	0.3670	0.61
30 - 35°S	2.1154	0.3993	0.61

CSIRO
Marine Laboratories
comprises

Division of Oceanography
Division of Fisheries Research

HEADQUARTERS
Castray Esplanade, Hobart, Tas
G.P.O. Box 1538, Hobart, Tas 7001,
Australia

QUEENSLAND LABORATORY
233 Middle Street, Cleveland, Qld
P.O. Box 120, Cleveland, Qld 4163

WESTERN AUSTRALIAN LABORATORY
Leach Street, Marmion, WA
P.O. Box 20, North Beach, WA 6020

ISSN 0725-4598